

# Pyridine nucleotide transhydrogenase PntAB is essential for optimal growth and photosynthetic integrity under low-light mixotrophic conditions in *Synechocystis* sp. PCC 6803

Jari Kämäräinen<sup>1\*</sup>, Tuomas Huokko<sup>1\*</sup>, Sanna Kreula<sup>1\*</sup>, Patrik R. Jones<sup>2</sup>, Eva-Mari Aro<sup>1</sup> and Pauli Kallio<sup>1</sup>

<sup>1</sup>Molecular Plant Biology, Department of Biochemistry, University of Turku, 20014 Turun Yliopisto, Finland; <sup>2</sup>Department of Life Sciences, Imperial College London, Sir Alexander Fleming Building, London, SW7 2AZ, UK

Authors for correspondence:

Eva-Mari Aro  
Tel: +358 2 333 5931  
Email: evaaro@utu.fi

Pauli Kallio  
Tel: +358 2 333 7913  
Email: pataka@utu.fi

Received: 17 February 2016  
Accepted: 25 October 2016

New Phytologist (2016)  
doi: 10.1111/nph.14353

**Key words:** cyanobacteria, low-light, mixotrophic, NAD(P)H, photobioreactor MC1000, photosynthetic machinery, PntAB, Transhydrogenase.

## Summary

- Pyridine nucleotide transhydrogenase (PntAB) is an integral membrane protein complex participating in the regulation of NAD(P)<sup>+</sup>:NAD(P)H redox homeostasis in various prokaryotic and eukaryotic organisms. In the present study we addressed the function and biological role of PntAB in oxygenic photosynthetic cyanobacteria capable of both autotrophic and heterotrophic growth, with support from structural three-dimensional (3D)-modeling.
- The *pntA* gene encoding the  $\alpha$  subunit of heteromultimeric PntAB in *Synechocystis* sp. PCC 6803 was inactivated, followed by phenotypic and biophysical characterization of the  $\Delta pntA$  mutant under autotrophic and mixotrophic conditions.
- Disruption of *pntA* resulted in phenotypic growth defects observed under low light intensities in the presence of glucose, whereas under autotrophic conditions the mutant did not differ from the wild-type strain. Biophysical characterization and protein-level analysis of the  $\Delta pntA$  mutant revealed that the phenotypic defects were accompanied by significant malfunction and damage of the photosynthetic machinery.
- Our observations link the activity of PntAB in *Synechocystis* directly to mixotrophic growth, implicating that under these conditions PntAB functions to balance the NADH:NADPH equilibrium specifically in the direction of NADPH. The results also emphasize the importance of NAD(P)<sup>+</sup>:NAD(P)H redox homeostasis and associated ATP:ADP equilibrium for maintaining the integrity of the photosynthetic apparatus under low-light glycolytic metabolism.

## Introduction

Controlled electron transfer through the reduction and oxidation of specific electron carriers is one of the core processes in cellular metabolism. In oxygen-evolving photosynthetic organisms such as *cyanobacteria*, light energy is used to extract electrons from H<sub>2</sub>O in order to reduce CO<sub>2</sub> for the production of organic carbon compounds. In heterotrophic metabolism, the primary flow of electrons takes place in the opposite direction, and the electrons derive from externally acquired reduced substrates, which provide the energy needed to drive cellular processes. Consequently, the relay of electrons in autotrophic cyanobacteria is fundamentally different from heterotrophic bacteria such as *Escherichia coli*, and directly linked with the regulation of the intracellular ratios of the different soluble electron carriers, as well as the enzyme components involved.

NAD(H) and NADP(H) are the most ubiquitous soluble electron/proton carriers in enzyme-catalyzed redox reactions in all living cells. The difference between these two molecules is the 2'

phosphate group in the adenine moiety ribose ring in NADP(H), which allows specific enzymes to distinguish between the two corresponding molecules. This reflects the different metabolic roles of NAD(H) and NADP(H), and is vital for the maintenance of cellular redox homeostasis; the intracellular ratio between the reduced and oxidized forms of the two electron carriers is typically different, and must be regulated independently. In most metabolic conditions, NADP(H) is used in reductive reactions and the NADP<sup>+</sup>:NADPH ratio is typically < 1, whereas NAD(H) is associated mainly with oxidative catabolic reactions with the NAD<sup>+</sup>:NADH ratio > 1. NADPH is the predominant form of reduced equivalents generated in photosynthesis, and expected to be abundantly available under autotrophic conditions. By contrast, under heterotrophic growth the complete breakdown of glucose via the Embden–Meyerhof–Parnas (EMP) pathway and the tricarboxylic acid (TCA) cycle generates primarily NADH. The redox balance under glycolytic conditions may be altered by redirecting the metabolic flux through alternative routes such as the oxidative pentose phosphate pathway (OPP) (You *et al.*, 2015) and Entner–Doudoroff (ED) pathway (Flamholz *et al.*, 2013; Chen *et al.*, 2016) which produce additional NADPH.

\*These authors contributed equally to this work.

*Pyridine nucleotide transhydrogenase* (PntAB; EC 1.6.1.2) is a specific integral membrane protein complex which has a direct role in the regulation of electron carrier redox balance by catalyzing energy-coupled electron transfer between NAD(H) and NADP(H) (Sauer *et al.*, 2004). PntAB is widely, yet very irregularly distributed in nature (Jackson, 2012), and it is located in the mitochondrial membrane in eukaryotes and in the outer cell membrane in heterotrophic bacteria. The enzyme couples the simultaneous reduction of NADP<sup>+</sup> and oxidation of NADH to the translocation of protons along the membrane proton gradient, which enables the intracellular [NADPH][NAD<sup>+</sup>]:[NADP<sup>+</sup>][NADH] ratios to reach levels up to >400 (Jackson, 2003, 2012). The physiological function, catalytic mechanism and structure of PntAB have been extensively studied in various heterotrophs (Sauer *et al.*, 2004; Jackson, 2012; Jackson *et al.*, 2015), but the biological role in prokaryotic oxygenic photosynthetic organisms (cyanobacteria) has remained elusive.

Although membrane-bound transhydrogenases from different organisms vary in their polypeptide composition and quaternary structure, the native enzyme always is composed of three distinct structural components: dI and dIII which bind NAD<sup>+</sup>:NADH and NADP<sup>+</sup>:NADPH, respectively, and dII which forms the integral membrane proton channel. Characteristically, these are arranged in two protomers (designated A and B) which form an asymmetric native dI-dII-dIII 'dimer' as summarized in detail by Jackson (2003) and Jackson *et al.* (2015). The enzymes can be grouped into four different categories based on the overall topology: In mammals the enzyme is a (1) single polypeptide without clearly defined  $\alpha$  and  $\beta$  regions, whereas the bacterial counterparts are characteristically heteromultimers composed of different arrangements of separate  $\alpha$  and  $\beta$  polypeptides. These enzymes are encoded by (2) two genes ( $\alpha$  and  $\beta$ ; i.e. *pntA* and *pntB*) as in *E. coli* or (3) three genes ( $\alpha 1$ ,  $\alpha 2$ ,  $\beta$ ) as in *Rhodospirillum rubrum* or *Thermus thermophilus*. In some parasites the enzyme is encoded as a (4) single polypeptide which contains both subunits  $\alpha$  and  $\beta$ . Accordingly, the number of the transmembrane helices in dII domains varies from one organism to another, and the enzyme spans the membrane altogether 12–14 times depending on the overall structure. Currently there are several partial transhydrogenase three-dimensional (3D) crystal structures available from different organisms. Most structures represent the individual, entire or partial, domains dI (from *E. coli*, *R. rubrum*, *T. thermophilus* and *Sinorhizobium meliloti*) and dIII (from *T. thermophilus*, *R. rubrum*, *Homo sapiens* and *Bos taurus*), whereas there is only a single crystal structure for the transmembrane domain dII (from *T. thermophilus*). In addition to the individual polypeptide/domain crystal structures, partial quaternary complex structures are available for PntAB from *T. thermophilus* (Leung *et al.*, 2015), *E. coli* (T. Johansson, A. Pedersen, J. Leckner & B. G. Karlsson, unpublished; NMR structure PDB accession number 2BRU) and *R. rubrum* (Bhakta *et al.*, 2007).

Thorough structural and functional characterization has revealed that transhydrogenases – despite the different topologies – employ a common binding-change mechanism, which couples the proton translocation to allosteric conformational changes upon substrate binding and release (see reviews of Jackson, 2012;

Jackson *et al.*, 2015). During the catalytic cycle the enzyme shifts between two alternative conformations: The *open conformation* allows substrate binding and product release in dI and dIII, whereas the *occluded conformation* brings the reacting species to appropriate orientation to allow the redox reaction to take place. The interconversion between the two alternative states is associated with proton translocation via the transmembrane dII, which transmits the structural change via the bound dIII to the dI interface. In the native quaternary structure the two dI-dII-dIII dimers shift in turn between the two alternative conformations. It has been suggested recently that this involves drastic movement of dIII between so-called *face-up* and *face-down* orientations, which allows the hydride transfer between NADH and NADP<sup>+</sup> and proton translocation across the membrane through dII, respectively (Jackson *et al.*, 2015).

Cyanobacteria harbor genes for the  $\alpha$  and  $\beta$  subunits of PntAB, but apart from a few indirect global transcript profiling (Ludwig & Bryant, 2011; Osanai *et al.*, 2011) and proteomic (Pisareva *et al.*, 2011) studies, the biological role of the enzyme has not been investigated in oxygenic photosynthetic prokaryotes. Here we address, from a bioinformatics viewpoint, the structural and evolutionary features of PntAB in *Synechocystis* sp. PCC 6803 (hereafter *Synechocystis*), and report the *in vivo* function of PntAB, with respect to growth and photosynthetic performance under autotrophic, mixotrophic and heterotrophic conditions, by comparing the  $\Delta pntA$  mutant and the WT strain.

## Materials and Methods

### General molecular biology methods

Standard molecular biology procedures and commercial kits (Qiagen, Hilden, Germany and NucleoSpin, Düren, Germany) were used for DNA plasmid isolation and manipulation. The enzymes and reagents were purchased from Thermo Scientific, Vilnius, Lithuania (Phusion polymerase), Fermentas (T4 DNA ligase) and New England BioLabs.

### Bacterial strains

DNA plasmid amplification and selection was carried out using *Escherichia coli* strain DH5 $\alpha$ . The cyanobacterial strain used for transhydrogenase inactivation studies was *Synechocystis* sp. PCC 6803 (WT).

### Inactivation construct for *slr1239* in *Synechocystis*

A DNA plasmid construct was designed for the disruption of the gene *slr1239* coding for the pyridine nucleotide transhydrogenase subunit  $\alpha$  (PntA) in *Synechocystis* by integration of a kanamycin resistance cassette (Km<sup>R</sup>) in the middle of the gene by homologous recombination. A DNA fragment spanning 500 bp on each side of the intended site of insertion was first PCR-amplified using isolated DNA of *Synechocystis* as template and *slr1239*-*SacI*-for and *slr1239*-*Bam*HI-rev (Table 1) as cloning primers. The resulting DNA fragment was subcloned as *SacI*-*Bam*HI into the

*E. coli* vector pUC19 (New England Biolabs, Ipswich, MA, USA). Km<sup>R</sup> (encoding aminoglycoside 3'-phosphotransferase originating from *Corynebacterium diphtheria*) was then amplified from the plasmid pCOLA-Duet-1 (Novagen) using primers Km<sup>R</sup>-*AvrII*-for and Km<sup>R</sup>-*AvrII*-rev (Table 1), and subcloned into the *AvrII* site in the pUC19-*slr1239* construct. The resulting construct named pUC19-*slr1239*::Km<sup>R</sup> was amplified in *E. coli* and used further for transformation into *Synechocystis*.

### Transformation into *Synechocystis* and confirmation of segregation

The integration construct pUC19 *slr1239*::Km<sup>R</sup> was transformed into *Synechocystis* using standard established protocols (Eaton-Rye, 2011), followed by selection on BG11 plates supplemented with kanamycin (gradual increase from 10 to 50 µg ml<sup>-1</sup>). Integration of the Km<sup>R</sup> cassette into the target gene *slr1239* and segregation of the mutant strain was verified with PCR from transformant colonies. The primers used in the colony PCR were *slr1239*-*SacI*-for and *slr1239*-*Bam*HI-rev (Table 1) and the expected fragment sizes were 2.3 kb for the mutant and 1 kb for the wild-type (WT), respectively.

### Culture media and standard growth conditions

*Escherichia coli* cells were cultured in Luria-Bertani medium (Tryptone 10 g l<sup>-1</sup>, NaCl, 10 g l<sup>-1</sup>, yeast extract, 5 g l<sup>-1</sup>) supplemented with the appropriate antibiotics using standard microbiology procedures. *Synechocystis* was cultivated in BG11 liquid medium (Stanier *et al.*, 1971) buffered with 10 mM TES-KOH (pH 8.0), with additional 5.5 mM glucose in the mixotrophic conditions. Precultures were carried out in 20 ml volume in 100 ml Erlenmeyer flasks in Sanyo culture chambers (100 rpm, 1% CO<sub>2</sub>, 30°C and 50 µmol photons m<sup>-2</sup> s<sup>-1</sup> continuous white light). All cell cultures used for strain characterization and analysis were carried out without antibiotics.

### Bioreactor cultures of *Synechocystis* and evaluation of phenotype

Comparison of the *Synechocystis* mutant *slr1239*::Km<sup>R</sup> (referred to as  $\Delta$ *pntA* from here on) and the WT growth rates were carried out using a photobioreactor Multi-Cultivator MC 1000 (Photon Systems Instruments, Brno, Czech Republic) equipped with eight parallel 100-ml growth chambers, aeration, temperature control,

**Table 1** PCR primers used in the work

<i>slr1239</i> - <i>SacI</i> -for 5'-	TAATGAGCTCATGGGGACGATTGATGACAATTTTGGC -3'
<i>slr1239</i> - <i>Bam</i> HI-rev 5'-	ATTAGGATCCCTTAAAGTCCAGCAGGAGAAATCCCC -3'
Km <sup>R</sup> - <i>AvrII</i> -for 5'-	ATATCCTAGGATGCCTATTTGTTATTTTCTAAATACATTCAAATAT -3'
Km <sup>R</sup> - <i>AvrII</i> -rev 5'-	ATATCCTAGGCTGAGCAATAACTAGCATAACCCCTT -3'

Restriction sites used for subcloning are underlined.

light control and automated optical density monitoring. Parallel 80-ml cultures were adjusted to the starting OD<sub>730 nm</sub> = 0.2 in BG11 and cultured for 6–7 d in ambient CO<sub>2</sub>, and the optical density was recorded every hour. The cultures were evaluated under six different light conditions (continuous white light 5, 20 and 50 µmol photons m<sup>-2</sup> s<sup>-1</sup> or diurnal sinusoidal rhythm with white light maximum 20, 50 and 200 µmol photons m<sup>-2</sup> s<sup>-1</sup> followed by 12 h dark period) with and without supplemented glucose (5.5 mM), added at the beginning of the growth experiment. In addition to 2–3 biological replicates in every run, each of the measurements was repeated 3–4 times.

For the biophysical measurements and Western analysis, the cells were cultivated in the presence and absence of 5.5 mM glucose under 12 h sinusoidal light (maximum light intensity of 50 µmol photons m<sup>-2</sup> s<sup>-1</sup>): dark cycles. The samples were collected at the midpoint of the light phase on d4 for immediate fluorescent and P700 absorbance measurements. For Western analysis the cells were pelleted, frozen in liquid nitrogen and stored at -20°C until use.

### Fluorescence induction and P700 absorbance

The Chl *a* fluorescence and P700 were recorded simultaneously from intact cells with pulse amplitude modulated fluorometer Dual-PAM-100 (Walz, Effeltrich, Germany). Before the measurements, the Chl *a* concentration of the samples was adjusted to 15 µg ml<sup>-1</sup> followed by dark-acclimation for 10 min. After recording  $F_0$  (fluorescence after turning on the measuring light), firing of a saturating pulse (5000 µmol photons m<sup>-2</sup> s<sup>-1</sup>, 300 ms) allowed determination of the maximal fluorescence ( $F_m^D$ ). Subsequent strong far red light (FR, 720 nm, 75 W m<sup>-2</sup>) was applied to preferentially excite photosystem I (PS I) and thus triggering a transition from State II to State I (Mullineaux & Allen, 1986; Kirilovsky, 2014), followed by a saturating pulse to record maximal fluorescence ( $F_m^{FR}$ ). After this, actinic light (50 µmol photons m<sup>-2</sup> s<sup>-1</sup>) was turned on and saturating pulses were applied every 20 s to monitor maximum fluorescence in light ( $F'_m$ ). The effective yield of photosystem II (PS II), Y(II), was calculated as  $(F'_m - F_s)/F'_m$ , and after 100 s of illumination, the average of five data points was calculated to compare the values between WT and the  $\Delta$ *pntA* mutant. The effective yield of PS I, Y(I), was calculated as  $Y(I) = (P'_m - P)/P_m$ . The Y(ND), donor side limitation of PS I, was calculated as  $P/P_m$ .  $F_m$  was recorded in the presence of 20 µM 3-(3,4-dichlorophenyl)-1,1-dimethylurea (DCMU).

### State transition analysis

In order to measure state transitions more precisely with a Dual-PAM fluorometer, the dark-acclimated cells were first illuminated with blue light (460 nm, 44 µmol photons m<sup>-2</sup> s<sup>-1</sup>) to induce State I. During illumination, saturating pulses were applied to monitor the maximal fluorescence in light ( $F'_m$ ). After 135 s the blue light was turned off and illumination was immediately continued with red light (620 nm, 50 µmol

photons  $\text{m}^{-2} \text{s}^{-1}$ ) to induce transition from State I to State II. After 215 s of red light illumination, light was again changed to blue to induce transition back to State I.

### Photosynthetic light response curves

Photosynthetic response to changing light intensities was evaluated by measuring rapid light response curves with a Dual-PAM fluorometer using a standard protocol of 60 s illumination periods of gradually increasing light intensity. To obtain the photosynthetic parameters, the saturating pulse was applied at the end of every light period. The maximum amount of P700<sup>+</sup> ( $P_m$ ) was determined with application of a saturation pulse after pre-illumination with strong FR light. The effective quantum yield of PS II, Y(II), and the donor side limitation of PS I, Y(ND) were calculated as described earlier.

### 77K fluorescence spectra

The fluorescence emission spectra at 77K were measured from intact cells using QE Pro-FL spectrofluorometer (Ocean Optics). The Chl *a* concentration of the samples was adjusted to  $7.5 \mu\text{g ml}^{-1}$ . Before measurements, the samples were frozen rapidly in liquid nitrogen and subsequently excited with the 580 nm or 440 nm light generated with a monochromator (Applied Photophysics Ltd; *f*/3.4 grating).

### Western blot analysis

Protein analysis by Western blotting was performed on total extracts of WT and  $\Delta pntA$  mutant cells grown under 12 h sinusoidal light (maximum light intensity of  $50 \mu\text{mol photons m}^{-2} \text{s}^{-1}$ ): 12 h dark cycles with and without 5.5 mM glucose. The proteins were isolated as described previously (Zhang *et al.*, 2009), separated in 12% (w/v) SDS-PAGE containing 6 M urea and transferred to polyvinylidene difluoride (PVDF) membrane (Immobilon-P; Millipore). Immunodetection was performed using protein-specific antibodies (Agrisera, Vännäs, Sweden). In addition, Western blot analysis was carried out for fractionated WT *Synechocystis* membrane samples in order to confirm the localization of PntAB in the cell. The membrane fractions were prepared as described previously (Zhang *et al.*, 2004).

### Homology modeling of PntAB quaternary structure

The amino acid sequences for *Synechocystis* PntA (*slr1239*) and PntB (*slr1434*) were obtained from the UniProt Knowledgebase (<http://www.uniprot.org>). The templates for modeling *Synechocystis* PntA and PntB were retrieved by BLAST through Protein Data Bank (PDB) (Altschul *et al.*, 1997, 2005) and selected based on highest identity (above 40% and 50%, respectively; 39/42% for the transmembrane structure). Thirteen templates were used for the modeling of the hydrophilic  $\alpha$  dI domain (PDB codes: 1X13, 1PTJ, 1L7D, 1HZZ, 2FRD, 2FSV, 1NM5, 2FR8, 1F8G, 4DIO, 4O9U, 4IZH, 4O93), three templates for the  $\alpha$  dII domain (PDB codes: 4O9U, 4O93, 4O9T) and 10 templates for

dIII/dII  $\beta$  domain (PDB codes: 2BRU, 1D4O, 1PTJ, 4O9U, 1DJL, 2FSV, 1E3T, 4J16, 1XLT, 1PNO). The number of transmembrane helices and the associated amino acids in the  $\alpha$  and  $\beta$  subunits were predicted with TMHMM server 2.0 (Krogh *et al.*, 2001), and modeled based on the only existing PDB crystal structure (*T. thermophilus*). The transmembrane helix 1 missing in the template structure was modeled based on the  $\alpha$  subunit transmembrane helices 2–4.

Homology models for PntA and PntB were assembled with MODELLER (Sali & Blundell, 1993). Five models were created for both PntA and PntB, out of which the best models were selected based on the highest assessment score and the lowest value of the objective function calculated by MODELLER for further analysis. Models were evaluated by MOLPROBITY (Chen *et al.*, 2010). Multiple sequence alignment comparison and models were visualized and analyzed with UCSF CHIMERA (Pettersen *et al.*, 2004).

### Phylogenetic analysis

Phylogenetic trees were assembled to compare the amino acid sequences of *Synechocystis* PntA and PntB against the corresponding homologs with 3D crystal structures available in PDB. The complete sequences were retrieved from PDB and UniProt Knowledgebase, and the comparison was carried out by running BLAST. Rooted phylogenetic tree were aligned in CLUSTAL OMEGA (Sievers *et al.*, 2011) and generated with iTOL (Letunic & Bork, 2007).

## Results

### Sequence analysis and structural model of PntAB in *Synechocystis*

Sequence analysis revealed that *Synechocystis* genome harbors genes coding for the heteromultimeric *pyridine nucleotide transhydrogenase* PntAB, which is composed of a 530 aa  $\alpha$  subunit (encoded by *pntA*; *slr1239*) and a 480 aa  $\beta$  subunit (encoded by *pntB*; *slr1434*). Although the primary structure appears to be rather well conserved in prokaryotes, the *Synechocystis* enzyme shares especially high amino acid sequence identity (often above 70%) with homologs in the cyanobacterial phylum. As the phylogenetic comparison against enzymes with available crystal structures illustrates (Fig. 1), the closest counterpart is the well-characterized PntAB from *E. coli* with 61% and 68% sequence identity to the  $\alpha$  and  $\beta$  subunits, respectively. Sequence identity with enzymes from other organisms found in PDB is 39–54% for  $\alpha$  and 42–54% for  $\beta$ . These enzymes were used as templates to predict the assembly of the individual polypeptides in the *Synechocystis* PntAB and their arrangement in the native quaternary structure as presented in Fig. 2.

Sequence comparisons with characterized homologs indicated that both subunits of the cyanobacterial PntAB are associated with substrate binding as well as anchoring the complex to the membrane (Fig. 2a,b). The N-terminal part of the  $\alpha$  subunit belongs to the group of short-chain dehydrogenases/reductases

**Fig. 1** Phylogenetic comparison of the *Synechocystis* pyridine nucleotide transhydrogenase PntA and PntB amino acid sequences against enzyme homologs with available crystal structures (Protein Data Bank). Amino acid sequence identities have been listed for the complete sequences as well as for the individual crystal structure domains. *E. coli*, *Escherichia coli*; *R. rubrum*, *Rhodospirillum rubrum*; *S. meliloti*, *Sinorhizobium meliloti*; *T. thermophilus*, *Thermus thermophilus* *B. taurus*, *Bos taurus*; *H. sapiens*, *Homo sapiens*.

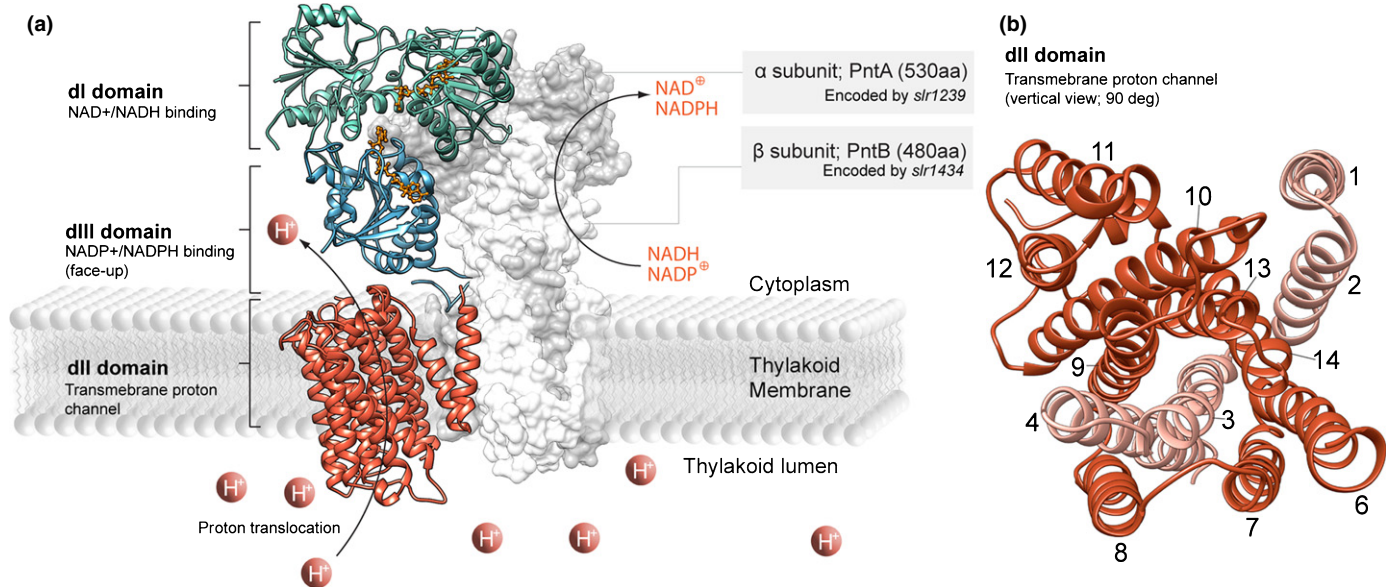
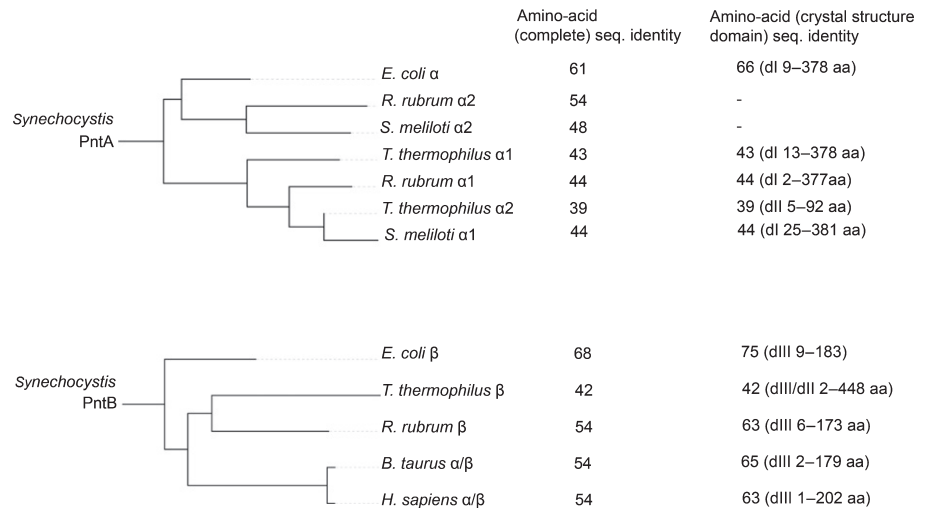


**Fig. 2** Quaternary structure model of *Synechocystis* pyridine nucleotide transhydrogenase (PntAB) assembled based on available crystal structures from six different organisms (template aa sequence identity for dI and dIII > 40% and > 50%, respectively, and for dII c. 30%). (a) The grey surface model in the background represents one of the two PntAB subunits, showing the α (PntA; darker grey) and β (PntB; lighter grey) polypeptides. The other heterodimer is represented as a cartoon model in the foreground, highlighting the interacting domains dI (green), dII (red), and dIII (blue) of α and β. (b) The modeled PntAB proton channel showing the transmembrane helices in dII viewed from the thylakoid lumen. The helices 1–4 (lighter red) represent the C-terminal end of the α subunit, and the helices 6–14 (darker red) constitute the N-terminal end of the β subunit. The first helix ('helix 5') of the β subunit identified in the primary prediction was excluded from the dII integral membrane structure because more detailed analysis suggested that it is more likely associated with the dI substrate-binding domain. The transmembrane helices 3, 9 and 13 are expected to form the core of the proton channel whereas the helices 4, 10 and 14 assemble as a surrounding bundle. The transmembrane helix 1 was modeled based on the available crystal structures for the helices 2–4.

(SDRs) and harbors the domain for NAD<sup>+</sup>: NADH binding (dI; predicted amino acids 1–421), whereas the hydrophobic C-terminal part constitutes the integral transmembrane domain (dII; predicted amino acids 422–521/four transmembrane helices). Initially, the transmembrane helix prediction led to the identification of a fifth putative integral helix in the α subunit (190–212 aa), but further comparison with the *E. coli* crystal structure suggested that this secondary structure element is more likely to be associated with the dI domain. In the β subunit the domains are arranged in an opposite order, and the C-terminal region is homologous to a highly conserved PNTB superfamily

with deoxyhypusine synthase (DHS)-like domain associated with NADP<sup>+</sup>: NADPH binding (dIII; predicted amino acids 263–480), whereas the N-terminal domain is part of the transmembrane proton conducting channel (dII; predicted amino acids 4–262/nine transmembrane helices).

### Disruption of the *pntA* gene in *Synechocystis*

The gene *pntA* coding for the α subunit of transhydrogenase PntAB in *Synechocystis* was inactivated by the insertion of a kanamycin resistance cassette by homologous recombination in

the middle of the open reading frame. The resulting kanamycin resistant transformant colonies were screened using colony PCR to confirm the presence of the resistance cassette in the *pntA* gene. Subsequently, the selected candidates of *Synechocystis pntA::Km<sup>R</sup>* ( $\Delta pntA$ ) were cultivated for several generations followed by PCR analysis to confirm segregation; The size of all obtained PCR fragments corresponded to the size of the disrupted gene (2.3 kb) whereas the presence of the WT *pntA* (1 kb) could not be detected (Fig. 3a). In addition, Western blot analysis using the PntA-specific antibody confirmed that the enzyme was not expressed in the mutant strain but could be detected in the WT strain at the expected size range (calculated weight 56 kDa) (Fig. 3b).

### Localization of PntAB in the thylakoid membrane

Western blot analysis was also performed on fractionated samples of WT *Synechocystis* cells to verify the localization of PntAB *in vivo*. As seen in Fig. 3(c), PntA was found almost exclusively in the thylakoid membrane fraction. A faint band also was observed in the plasma membrane fraction, but this was expected to derive from incomplete fractionation rather than differential localization of the enzyme in the native context.

### PntA deletion mutant has no growth phenotype under autotrophic conditions

The segregated *Synechocystis*  $\Delta pntA$  was expected to be fully deficient of transhydrogenase activity specific to PntAB. The strain, however, did not show any phenotypic differences compared with WT under the standard autotrophic culture conditions (Figs 4, 5, dashed lines): under different intensities of continuous or diurnal light in BG11 medium, the growth and the physical appearance of the two strains appeared to be identical.

### A conditional $\Delta pntA$ phenotype appears in the presence of glucose

Contrary to autotrophic growth, a phenotypic difference between the  $\Delta pntA$  mutant strain and the WT was observed when the

culture medium was supplemented with glucose (5.5 mM) (Figs 4, 5, solid lines); Under various mixotrophic conditions the growth rate of the  $\Delta pntA$  mutant strain was clearly slower in comparison to WT (Figs 4c, 5b,c). Further supporting the direct link to glycolytic metabolism, the difference in growth rate between the two strains disappeared after glucose was used up from the growth medium.

### PntAB activity is particularly important under low-light mixotrophic growth conditions

In addition to the presence of glucose, the phenotypic growth defects of the *Synechocystis*  $\Delta pntA$  mutant were highly dependent on the light conditions. There was no apparent difference between the mutant and the WT strain when grown under 20 and 50  $\mu\text{mol photons m}^{-2} \text{s}^{-1}$  continuous light (Fig. 4a,b) or in diurnal sinusoidal rhythm with maximum intensity 200  $\mu\text{mol photons m}^{-2} \text{s}^{-1}$  (Fig. 5a). However, under lower light the growth of the  $\Delta pntA$  mutant was significantly impaired (Figs 4c, 5b,c). This was apparent during the light-phase of the sinusoidal diurnal rhythm with maximum intensity 50  $\mu\text{mol photons m}^{-2} \text{s}^{-1}$  (Fig. 5b), as well under the lowest light intensities in continuous light (5  $\mu\text{mol photons m}^{-2} \text{s}^{-1}$ ) (Fig. 4c) and sinusoidal rhythm (maximum 20  $\mu\text{mol photons m}^{-2} \text{s}^{-1}$ ) (Fig. 5c), where the cells could no longer sustain mixotrophic growth in the absence of PntAB.

### Photosynthetic characterization of the $\Delta pntA$ mutant under mixotrophic growth conditions

Photosynthetic properties of the *Synechocystis*  $\Delta pntA$  strain were studied in order to understand the underlying mechanisms for the observed growth defects under mixotrophic low-light conditions. Chl *a* fluorescence analysis of dark-acclimated  $\Delta pntA$  cells, carried out with Dual-PAM fluorometer, demonstrated significantly higher  $F_0$  intensity compared with WT cells (Fig. 6a). In addition, the maximal fluorescence ( $F_m^{\text{FR}}$ ) was clearly reduced in the  $\Delta pntA$  mutant (Fig. 6a). Analysis of the maximum Chl *a* fluorescence in light ( $F'_m$ ) revealed *c.* 65% lower effective yield of PS II, Y(II), in the  $\Delta pntA$  mutant compared with WT (Fig. 6b). This was in line with the maximum quantum yield of PS II ( $F_v/F_m$ ) measured in the presence of 20  $\mu\text{M}$  DCMU, which was 55% smaller in the  $\Delta pntA$  mutant compared with WT (Table 2). In parallel, *pntA* inactivation caused an increase in the donor side limitation of PS I, Y(ND) (Fig. 6c), whereas the maximal amount of oxidizable P700 ( $P_m$ ) in  $\Delta pntA$  was 33% smaller than in WT (Table 2). Nevertheless, the effective yield of PS I, Y(I), was not significantly impaired in response to *pntA* deletion (Supporting Information Fig. S1).

Because the  $F_m^{\text{FR}}$  and  $F'_m$  parameters in the  $\Delta pntA$  mutant did not differ from the value of the  $F_m^{\text{D}}$  parameter, unlike in WT (Fig. 6a), we decided to assess the capability of the mutant to perform state transitions, which are essential for balancing the absorbed light energy between the two photosystems. As shown in Fig. 6(d), the  $\Delta pntA$  mutant exhibited impaired state transitions to such an extent that the cells seemed to be almost locked in State II.

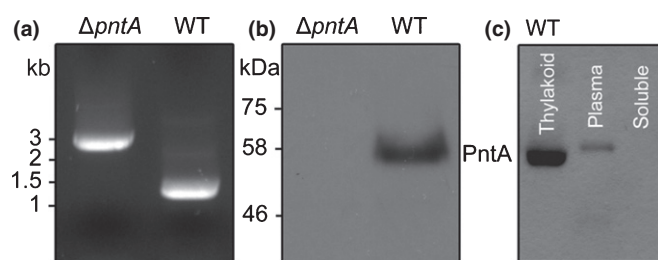


**Fig. 3** PCR and Western blot analysis of the *Synechocystis*  $\Delta pntA$  vs wild-type (WT). (a) Confirmation of *pntA* disruption and segregation in  $\Delta pntA$  mutant by colony PCR showing the presence of the kanamycin resistance cassette insert in *slr1239* (expected size 2.3 kb) in reference to the WT control (expected size 1 kb). (b) Western blot analysis of total protein extracts from the  $\Delta pntA$  mutant and the WT strain immunoblotted with a PntA-specific antibody (calculated molecular weight 65 kDa). (c) Corresponding Western blot analysis of WT fractions (thylakoid membrane, plasma membrane and soluble).

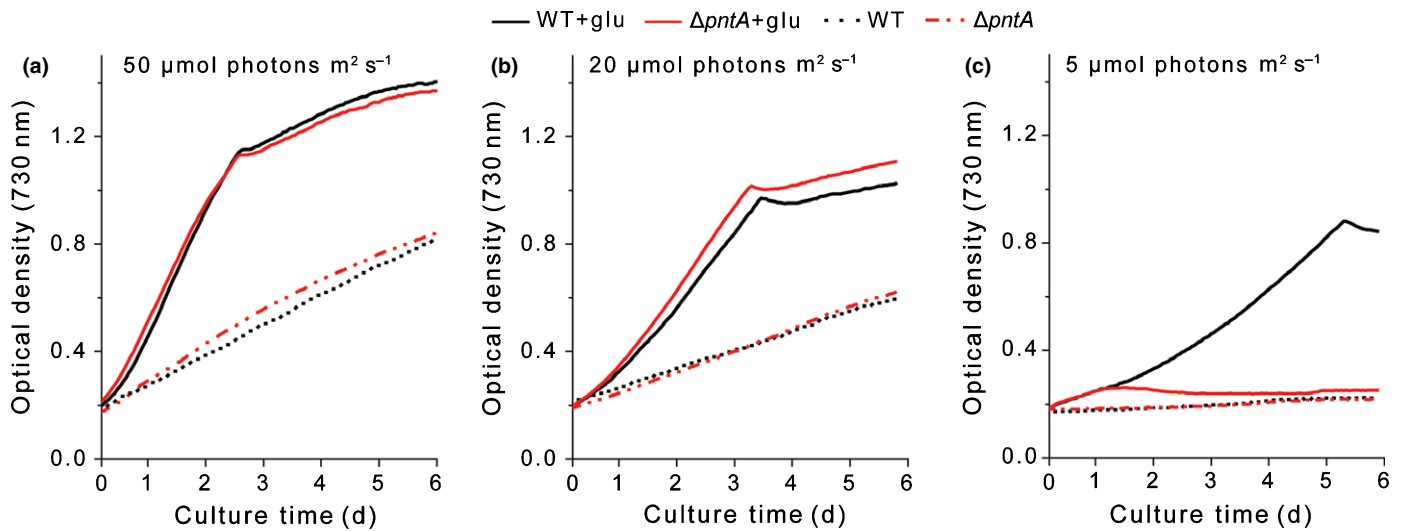


**Fig. 4** Growth of the *Synechocystis*  $\Delta pntA$  mutant (red line) vs wild-type (WT) strain (black line) under continuous light in the presence of 5.5 mM glucose (solid line) and in autotrophic conditions (dashed line). The cultures were monitored for 6 d in a photobioreactor MC1000 (BG11 and ambient  $\text{CO}_2$ ) under continuous light: (a)  $50 \mu\text{mol photons m}^{-2} \text{s}^{-1}$  light, (b)  $20 \mu\text{mol photons m}^{-2} \text{s}^{-1}$  light, (c)  $5 \mu\text{mol photons m}^{-2} \text{s}^{-1}$  light. The presented growth curves are representatives of parallel biological culture replicates ( $n = 2-3$ ). Leveling of the growth curves under mixotrophic conditions is expected to indicate the point of glucose depletion.

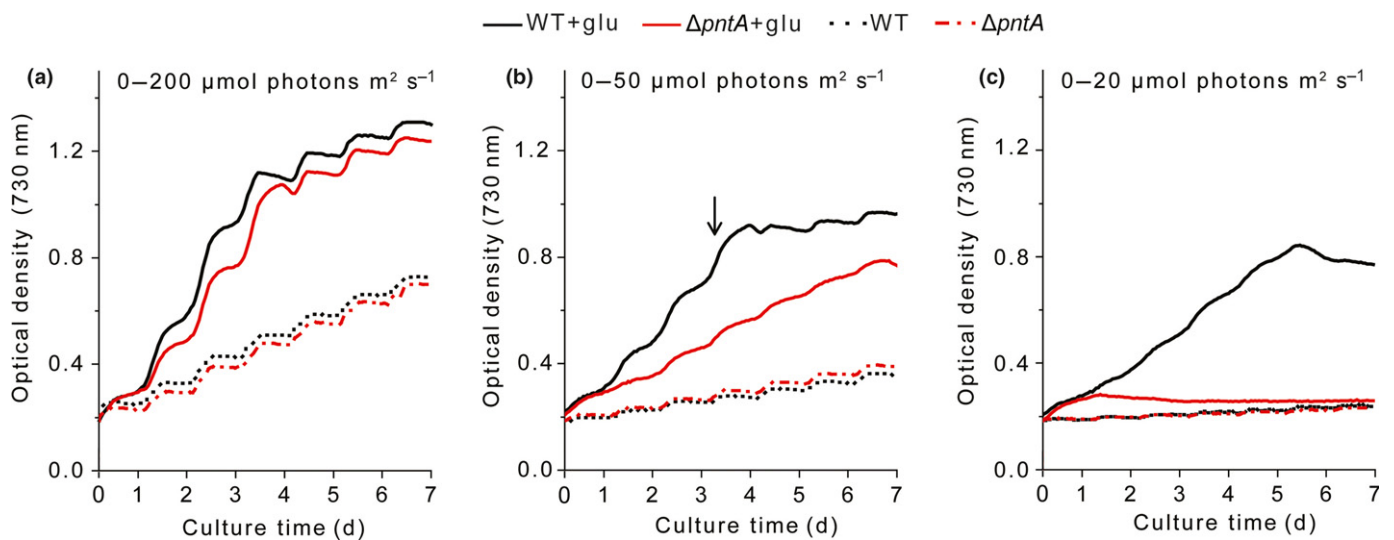


**Fig. 5** Growth of the *Synechocystis*  $\Delta pntA$  mutant (red line) vs wild-type (WT) strain (black line) under day–night rhythm. The cultures were monitored in the presence of 5.5 mM glucose (solid line) and under autotrophic conditions (dashed line) in a photobioreactor MC1000 (BG11 and ambient  $\text{CO}_2$ ) for 7 d under 12 h sinusoidal day : night cycles with white light maximum (a)  $0-200 \mu\text{mol photons m}^{-2} \text{s}^{-1}$  light, (b)  $0-50 \mu\text{mol photons m}^{-2} \text{s}^{-1}$  light, (c)  $0-20 \mu\text{mol photons m}^{-2} \text{s}^{-1}$  light. The arrow in (b) indicates the time-point at which the samples were collected for biochemical and biophysical analyses. Leveling of the curves towards the end of cultures is expected to indicate the point of glucose depletion. The presented growth curves are representatives of parallel biological culture replicates ( $n = 3-4$ ).

The reason for the observed low effective yield of PS II in the  $\Delta pntA$  mutant (Fig. 6b) was investigated further by evaluating the possibility of functional defects in PSII or a decrease in the amount of PSII complexes. The 77K fluorescence emission spectra excited with 440 nm light (Chl *a* excitation) showed a lower emission originating from PS II (685 and 695 nm) in the  $\Delta pntA$  strain as compared with WT (Fig. 7a), indicating a reduction in the PS II : PS I ratio. In parallel, excitation of the cells with 580 nm light (phycobilisome excitation) resulted in significantly

higher emission peaks originating both from phycobilisomes (*c.* 655 nm) and the terminal emitter (685 nm) in the  $\Delta pntA$  mutant cells as compared with WT (Fig. 7b), which together with high  $F_0$  intensity (Fig. 6a) provided compelling evidence in support of the detachment of phycobilisomes from PSII in the  $\Delta pntA$  mutant. This also was likely to be connected with the impaired state transitions (van Thor *et al.*, 1998; Minagawa & Takahashi, 2004; Mullineaux & Emlyn-Jones, 2005) in PntAB-deficient cells (Fig. 6d).

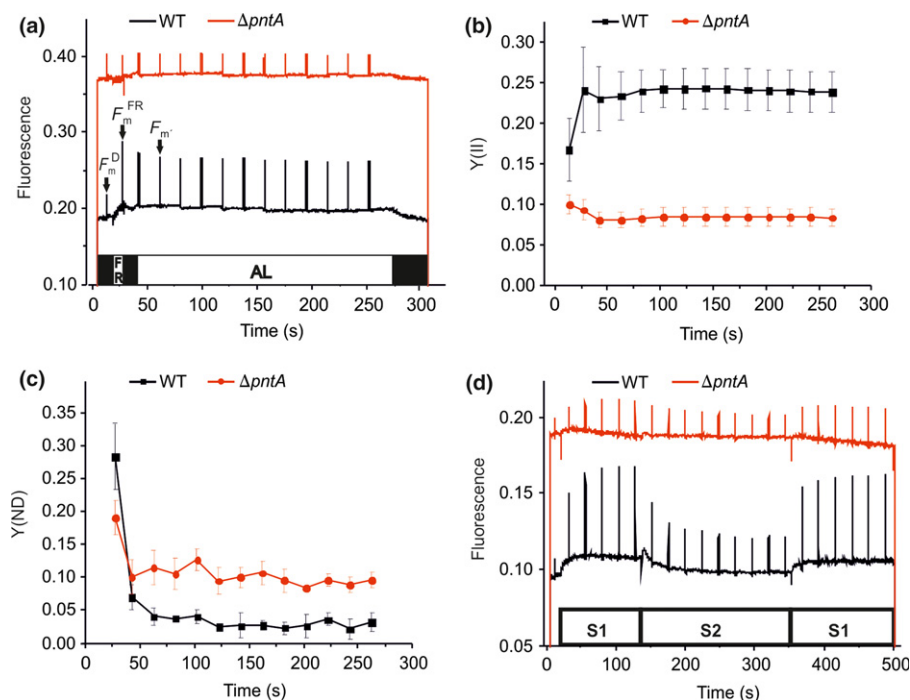


**Fig. 6** Photosynthetic characterization of the *Synechocystis*  $\Delta pntA$  mutant (red line) and the wild-type (WT) strain (black line) grown in the presence of glucose (see Fig. 5b). (a) Fluorescence analysis: Fluorescence was recorded upon dark acclimation (black bars), under far red light (FR) and under actinic light (AL) ( $50 \mu\text{mol photons m}^{-2} \text{s}^{-1}$ ). Saturating pulses were fired to record maximal fluorescence 'in darkness' ( $F_m^D$ ), under the FR background ( $F_m^{FR}$ ) and under illumination ( $F_m'$ ). Samples were dark-acclimated for 10 min before each measurement and the Chl *a* concentration was adjusted to  $15 \mu\text{g ml}^{-1}$ . (b) Photosystem II (PS II) yield,  $Y(II)$ , under illumination. Mean  $\pm$  SD,  $n = 3$ . (c) Donor side limitation of photosystem I (PS I),  $Y(ND)$ , under illumination. Mean  $\pm$  SD,  $n = 3$ . (d) State transition kinetics in WT and the  $\Delta pntA$  mutant. Chl *a* concentration was adjusted to  $7.5 \mu\text{g ml}^{-1}$  and samples were dark-acclimated for 10 min before measurements. Cells were exposed to blue light (S1;  $460 \text{ nm}$ ,  $44 \mu\text{mol photons m}^{-2} \text{s}^{-1}$ ), then to red light (S2;  $620 \text{ nm}$ ,  $50 \mu\text{mol photons m}^{-2} \text{s}^{-1}$ ) and again to blue light (S1).

### Photosynthetic protein content in WT and the $\Delta pntA$ mutant under mixotrophic conditions

The  $\Delta pntA$  mutant and WT were further compared in respect to the relative amounts of PSI and PSII at the protein level using Western blot analysis. When the strains were grown without glucose, there were no apparent quantitative differences in the proteins D1, PsaB, RbcL or CytF (Fig. 8). By contrast, when grown in the presence of glucose, the quantities of D1, RbcL and PsaB were 30%, 40% and 20% less abundant, respectively, in the  $pntA$  mutant as compared with WT. The amount of CytF remained unchanged.

### Photosynthetic dynamics of the $\Delta pntA$ mutant upon changing light intensities

The response of the  $\Delta pntA$  mutant to changing light intensities was evaluated by measuring rapid light response curves with Dual-PAM fluorometer. In darkness, as well as at low light intensities from  $c. 10$  to  $130 \mu\text{mol photons m}^{-2} \text{s}^{-1}$ , the effective yield of PS II,  $Y(II)$  was significantly lower in the  $\Delta pntA$  mutant than in WT (Fig. 9a). In agreement, the donor side limitation of PS I,  $Y(ND)$  was higher in the  $\Delta pntA$  mutant (Fig. 9b). Interestingly, these responses recorded at low light intensities became gradually alleviated upon increasing the light intensity, in analogy to the observed phenotypic growth defects of the  $\Delta pntA$  mutant (Figs 4, 5).

**Table 2** Photosynthetic parameters of the *Synechocystis*  $\Delta pntA$  mutant and the wild-type (WT) strain grown in the presence of glucose (see Fig. 5b):  $F_v/F_m$ , maximum quantum yield of photosystem II (PS II) and  $P_m$ , the maximum amount of oxidizable P700

	WT	$\Delta pntA$
$F_v/F_m$	$0.38 \pm 0.03$	$0.17 \pm 0.02$
$P_m$	$0.09 \pm 0.01$	$0.06 \pm 0.01$

Mean  $\pm$  SD,  $n = 3$ .

### Discussion

Intracellular NAD(H): NADP(H) redox balance is fundamentally different between autotrophic and heterotrophic organisms, which is reflected in the native function of the pyridine nucleotide transhydrogenase (PntAB). This study addressed the biological role of PntAB in the cyanobacterium *Synechocystis* sp. PCC 6803, which is capable of autotrophic, mixotrophic and heterotrophic metabolism. Apart from elucidation of the role of PntAB in different growth modes in cyanobacteria, understanding the function is relevant also from a bioengineering viewpoint, as overexpressed enzymes in heterologous pathways must be constantly supplied with appropriate soluble cofactors *in vivo* to allow efficient metabolic flux towards the target products (Angermayr *et al.*, 2012).

**Fig. 7** 77K fluorescence emission spectra of the *Synechocystis*  $\Delta pntA$  mutant (red line) and the wild-type (WT) strain (black line) when cells were excited with (a) 440 nm light and (b) 580 nm light. Cells were grown in the presence of glucose (see Fig. 5b).

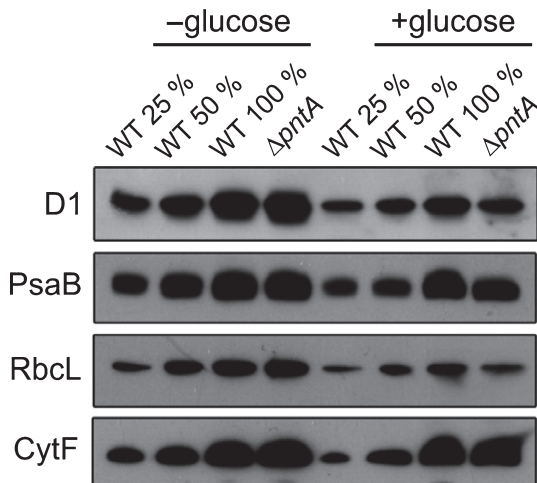
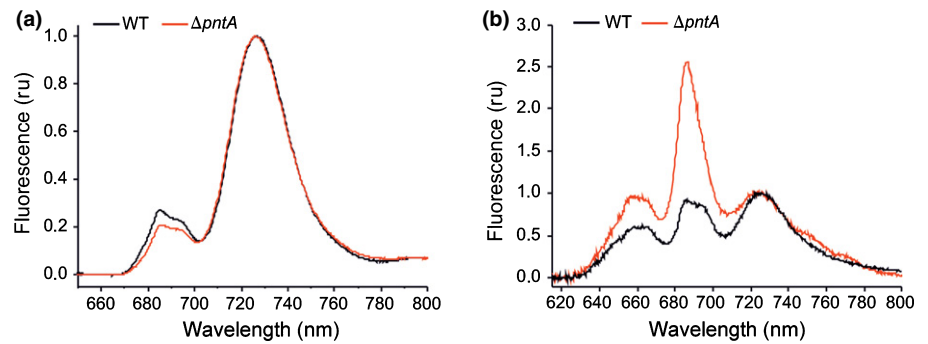


**Fig. 8** Western blot protein analysis of the *Synechocystis*  $\Delta pntA$  mutant and the wild-type (WT) strain. The cells were cultivated under 12 h sinusoidal light (maximum light intensity of  $50 \mu\text{mol photons m}^{-2} \text{s}^{-1}$ ); dark cycles with and without 5.5 mM glucose (see Fig. 5b). The samples were loaded on the basis of total protein concentration.

### Model of the PntAB transhydrogenase in the thylakoid membrane of *Synechocystis*; role of subunits and the catalytic function

PntAB is an integral membrane protein complex, which uses the membrane proton gradient to drive the catalytic hydride transfer between the two nicotinamide dinucleotide cofactors NAD(H) and NADP(H). As confirmed by specific antibody detection of PntA in fractionated *Synechocystis* cell samples (Fig. 3c), the enzyme is located in the thylakoid membrane, in agreement with earlier mass spectrometry-based proteomics studies (Pisareva *et al.*, 2011). According to the common catalytic mode and the findings presented in this study, PntAB in *Synechocystis* thus transfers protons along the gradient from the thylakoid lumen into the cytoplasm, while catalyzing the concomitant hydride transfer from NADH to NADP<sup>+</sup> on the cytoplasmic side.

Based on sequence analysis, PntAB in *Synechocystis* is composed of two separate subunits  $\alpha$  (PntA) and  $\beta$  (PntB), encoded by *pntA* (*slr1239*) and *pntB* (*slr1434*), which assemble together as a PntAB heterodimer. In the native quaternary structure two of these protomers further join together as the biologically active conformation  $\alpha_2\beta_2$ . As illustrated by the 3D structural model

(Fig. 2a,b) predicted using available crystal structures (Fig. 1), each PntAB protomer in *Synechocystis* has three distinct functional domains dI, dII and dIII. The integral membrane domain (dII) which constitutes the proton channel is composed of the C-terminal part of PntA (four transmembrane helices) and the N-terminal part of PntB (nine transmembrane helices) (Fig. 2b). Also, the native quaternary conformation responsible for substrate binding and the catalytic redox reaction requires both polypeptides (dI in PntA and dIII in PntB) (Fig. 2a), which clearly implies that neither PntA nor PntB is indispensable, and deletion of either of the corresponding genes would render the enzyme inactive.

### PntAB is needed specifically under low-light mixotrophic conditions

When grown autotrophically, the  $\Delta pntA$  mutant could not be distinguished from the wild-type (WT) based on growth (Figs 4, 5; dashed lines). However, under sufficiently low light intensities in the presence of glucose, the growth of the mutant was significantly impaired (Figs 4c, 5b,c, solid lines). This phenotypic behavior revealed a direct link between the native transhydrogenase activity and the capacity of *Synechocystis* to efficiently use supplied glucose. In line with this, enhanced expression of sugar catabolic genes was shown previously to increase the expression of both *pntA* and *pntB* in *Synechocystis* (Osana *et al.*, 2011). The fact that the phenotypic growth defects occurred specifically under low light implied that PntAB is especially important when the cell metabolism relies mainly on externally obtained carbohydrate substrates and the contribution of photosynthesis is at minimum. This effect was most evident during the light-phase of the sinusoidal day–night cycles when the total amount of light was too low for efficient photosynthetic growth (Fig. 5b), and under the lowest constant (Fig. 4c) and sinusoidal (Fig. 5c) light intensities which could no longer sustain mixotrophic growth of the  $\Delta pntA$  mutant. This emphasized the particular importance of PntAB for the capacity of cells to grow at the interphase of mixotrophic and heterotrophic metabolic modes in natural growth environments.

### Physiological role of PntAB

Phenotypic and biophysical characterization of the *Synechocystis*  $\Delta pntA$  mutant strain carried out in this study linked the

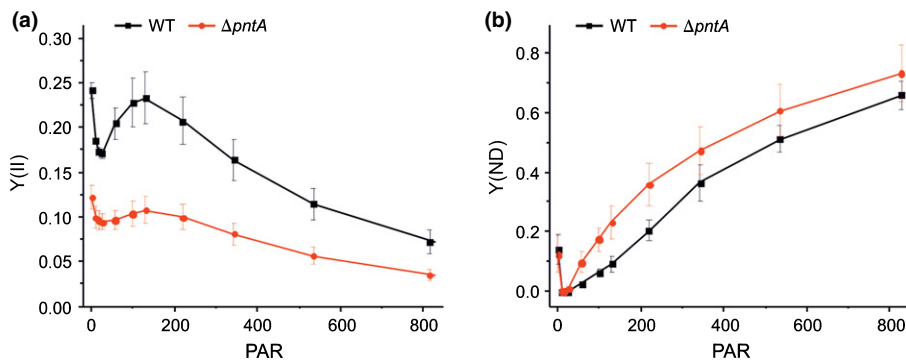


**Fig. 9** Rapid light curves of the *Synechocystis*  $\Delta pntA$  mutant (red line) and the wild-type (WT) strain (black line) grown in the presence of glucose (see Fig. 5b). (a) Photosystem II (PS II) yield, Y(II) and (b) Donor side limitation of photosystem I (PS I), Y(ND). PAR, photosynthetically active radiation ( $\mu\text{mol photons m}^{-2} \text{s}^{-1}$ ). Mean  $\pm$  SD,  $n = 3$ .

biological function of PntAB specifically to low-light mixotrophic growth. Under these conditions, the breakdown of glucose via the OPP pathway in *Synechocystis* has been shown to be marginal, and the carbon flux is expected to proceed mainly through the EMP pathway (You *et al.*, 2014). Thus, the optimal growth of *Synechocystis* is dependent on PntAB specifically when the generation of NADPH from both photosynthesis and glycolytic metabolism is limited, and the intracellular NADH:NADPH ratio is high. This suggests that the physiological role of PntAB in *Synechocystis* is to balance the NADH:NADPH equilibrium specifically in the direction of NADPH, in analogy to the reported function of the enzyme in *E. coli* (Sauer *et al.*, 2004). Consequently, PntAB acts to keep the intracellular NADP<sup>+</sup>:NADPH ratio low to provide reductive power for carbon assimilation and other metabolic reactions, such as amino acid and fatty acid biosynthesis or glutathione reduction in the absence of sufficient NADPH from photosynthesis. At the same time, PntAB keeps the NAD<sup>+</sup>:NADH ratio sufficiently high to sustain oxidative metabolism, for example, to allow the breakdown of glucose to continue. Notably, there is no clear difference in the growth between the WT and the  $\Delta pntA$  mutant during the dark phase of the day-night cycle (Fig. 5a,b). This may be explained by the significant metabolic flux via the OPP pathway in *Synechocystis* under fully heterotrophic conditions (Yang *et al.*, 2002; You *et al.*, 2015), which generates sufficient NADPH and thus alleviates the need for PntAB activity. From another perspective, these findings also imply that under mixotrophic conditions the NADPH-producing OPP pathway or the ED pathway cannot compensate for the lack of the transhydrogenase activity in the *Synechocystis*  $\Delta pntA$  mutant.

Failure to maintain favorable NAD(P)<sup>+</sup>:NAD(P)H redox equilibrium is expected to have serious consequences on the intracellular ATP:ADP balance also (Kramer & Evans, 2011). This is primarily because the respiratory ATP production via the NDH-1 electron transfer complex in cyanobacteria is dependent, albeit indirectly, specifically on NADPH (Thomas *et al.*, 2006; Peltier *et al.*, 2016; Shikanai & Aro, 2016). Thus, under the low-light mixotrophic conditions when photosynthetic production of NADPH is low, and the capacity of the  $\Delta pntA$  mutant to produce NADPH via glycolytic metabolism is compromised, the respiratory ATP production is likely to be limited. At the same time, the flux from glucose breakdown to the TCA cycle is negligible during mixotrophic growth (You *et al.*, 2014), thus further reducing the capacity of the cell to generate ATP.

The limited ATP production is a likely reason for the observed damage of the photosynthetic apparatus in the  $\Delta pntA$  mutant. PSII is known to be prone to photodamage even under low-light conditions (Tyystjärvi & Aro, 1996) and requires constant repair (Aro *et al.*, 1993). Sustainable PSII damage occurs if the rate of repair, directly requiring ATP, cannot be maintained in pace with the damage – the condition most likely faced by the  $\Delta pntA$  mutant under mixotrophic low-light growth conditions. Accordingly, we found significant damage and malfunction of the PSII electron transfer, the loss of PSII proteins, as well as detachment of phycobilisomes, and impaired capacity for state transitions in the  $\Delta pntA$  mutant (Figs 6–8). Deletion of *pntA* thus seems to have an indirect effect on the growth through the inactivation of the photosynthetic machinery: reduction of light energy capture by phycobilisomes, together with primary damage to PSII and consequent secondary damage on PSI, compromise the efficient use of photosynthetic light reactions for optimal mixotrophic growth of the  $\Delta pntA$  mutant. These problems were overcome by increasing the light intensity (Figs 4a,b, 5a), demonstrating that PntAB is dispensable when photosynthetic production of NADPH (and ATP) is sufficient.

Taken together, our results suggest that under low-light mixotrophic growth conditions, the majority of NADPH in *Synechocystis* is produced by PntAB. The enzyme appears to have a direct effect on cellular redox balance via glycolytic metabolism, and an indirect effect on the maintenance of the photosynthetic machinery, thus serving as a link between the two metabolic modes when the availability of light is limited.

## Acknowledgements

Our research was financially supported by Tekes (LiF project no. 40128/2014), the Academy of Finland (project nos. 271832, 273870, 272424 and 253269), and Emil Aaltonen Foundation. Sincere thanks to Martti Tolvanen for assistance in PntAB modeling and Yagut Allahverdiyeva for advice in biophysical analysis.

## Author contributions

P.K. and E-M.A., with P.R.J. at a very initial stage, planned and designed the research; J.K., T.H., S.K., E-M.A. and P.K. performed experiments/analyzed and interpreted data; and J.K., T.H., S.K., E-M.A. and P.K. wrote the manuscript.

## References

- Altschul SF, Madden TL, Schäffer AA, Zhang J, Zhang Z, Miller W, Lipman DJ. 1997. Gapped BLAST and PSI-BLAST: a new generation of protein database search programs. *Nucleic Acids Research* 25: 3389–3402.
- Altschul SF, Wootton JC, Gertz EM, Agarwala R, Morgulis A, Schäffer AA, Yu YK. 2005. Protein database searches using compositionally adjusted substitution matrices. *FEBS Journal* 272: 5101–5109.
- Angermayr SA, Paszota M, Hellingwerf KJ. 2012. Engineering a cyanobacterial cell factory for production of lactic acid. *Applied and Environmental Microbiology* 78: 7098–7106.
- Aro EM, Virgin I, Andersson B. 1993. Photoinhibition of photosystem II. Inactivation, protein damage and turnover. *Biochimica et Biophysica Acta* 1143: 113–134.
- Bhakta T, Whitehead SJ, Snaith JS, Dafforn TR, Wilkie J, Rajesh S, White SA, Jackson JB. 2007. Structures of the d12dIII1 complex of proton-translocating transhydrogenase with bound, inactive analogues of NADH and NADPH reveal active site geometries. *Biochemistry* 46: 3304–3318.
- Chen VB, Arendall WB, Headd JJ, Keedy DA, Immormino RM, Kapral GJ, Murray LW, Richardson JS, Richardson DC. 2010. MolProbity: all-atom structure validation for macromolecular crystallography. *Acta Crystallographica. Section D, Biological Crystallography* 66: 12–21.
- Chen X, Schreiber K, Appel J, Makowka A, Fährnich B, Roettger M, Hajirezaei MR, Sönnichsen FD, Schönheit P, Martin WF *et al.* 2016. The Entner-Doudoroff pathway is an overlooked glycolytic route in cyanobacteria and plants. *Proceedings of the National Academy of Sciences, USA* 113: 5441–5446.
- Eaton-Rye JJ. 2011. Construction of gene interruptions and gene deletions in the cyanobacterium *Synechocystis* sp. strain PCC 6803. *Methods in Molecular Biology* 684: 295–312.
- Flamholz A, Noor E, Bar-Even A, Liebermeister W, Milo R. 2013. Glycolytic strategy as a tradeoff between energy yield and protein cost. *Proceedings of the National Academy of Sciences, USA* 110: 10039–10044.
- Jackson JB. 2003. Proton translocation by transhydrogenase. *FEBS Letters* 555: 176–177.
- Jackson JB. 2012. A review of the binding-change mechanism for proton-translocating transhydrogenase. *Biochimica et Biophysica Acta* 1817: 1839–1846.
- Jackson JB, Leung JH, Stout CD, Schurig-Briccio LA, Gennis RB. 2015. Review and hypothesis. New insights into the reaction mechanism of transhydrogenase: swivelling the dIII component may gate the proton channel. *FEBS Letters* 589: 2027–2033.
- Kirilovsky D. 2014. Modulating energy arriving at photochemical reaction centers: orange carotenoid protein-related photoprotection and state transitions. *Photosynthesis Research* 126: 3–17.
- Kramer DM, Evans JR. 2011. The importance of energy balance in improving photosynthetic productivity. *Plant Physiology* 155: 70–78.
- Krogh A, Larsson B, von Heijne G, Sonnhammer EL. 2001. Predicting transmembrane protein topology with a hidden Markov model: application to complete genomes. *Journal of Molecular Biology* 305: 567–580.
- Letunic I, Bork P. 2007. Interactive Tree Of Life (iTOL): an online tool for phylogenetic tree display and annotation. *Bioinformatics* 23: 127–128.
- Leung JH, Schurig-Briccio LA, Yamaguchi M, Moeller A, Speir JA, Gennis RB, Stout CD. 2015. Structural biology. Division of labor in transhydrogenase by alternating proton translocation and hydride transfer. *Science* 347: 178–181.
- Ludwig M, Bryant DA. 2011. Transcription profiling of the model Cyanobacterium *Synechococcus* sp. strain PCC 7002 by Next-Gen (SOLiD™) sequencing of cDNA. *Frontiers in Microbiology* 2: 41.
- Minagawa J, Takahashi Y. 2004. Structure, function and assembly of Photosystem II and its light-harvesting proteins. *Photosynthesis Research* 82: 241–263.
- Mullineaux CW, Allen JF. 1986. The state 2 transition in the cyanobacterium *Synechococcus* 6301 can be driven by respiratory electron flow into the plastoquinone pool. *FEBS Letters* 205: 155–160.
- Mullineaux CW, Emllyn-Jones D. 2005. State transitions: an example of acclimation to low-light stress. *Journal of Experimental Botany* 56: 389–393.
- Osana T, Oikawa A, Azuma M, Tanaka K, Saito K, Hirai MY, Ikeuchi M. 2011. Genetic engineering of group 2 sigma factor SigE widely activates expressions of sugar catabolic genes in *Synechocystis* species PCC 6803. *Journal of Biological Chemistry* 286: 30962–30971.
- Peltier G, Aro EM, Shikanai T. 2016. NDH-1 and NDH-2 plastoquinone reductases in oxygenic photosynthesis. *Annual Review of Plant Biology* 67: 55–80.
- Petterson EF, Goddard TD, Huang CC, Couch GS, Greenblatt DM, Meng EC, Ferrin TE. 2004. UCSF Chimera – a visualization system for exploratory research and analysis. *Journal of Computational Chemistry* 25: 1605–1612.
- Pisareva T, Kwon J, Oh J, Kim S, Ge C, Wieslander A, Choi JS, Norling B. 2011. Model for membrane organization and protein sorting in the cyanobacterium *Synechocystis* sp. PCC 6803 inferred from proteomics and multivariate sequence analyses. *Journal of Proteome Research* 10: 3617–3631.
- Sali A, Blundell TL. 1993. Comparative protein modelling by satisfaction of spatial restraints. *Journal of Molecular Biology* 234: 779–815.
- Sauer U, Canonaco F, Heri S, Perrenoud A, Fischer E. 2004. The soluble and membrane-bound transhydrogenases UdhA and PntAB have divergent functions in NADPH metabolism of *Escherichia coli*. *Journal of Biological Chemistry* 279: 6613–6619.
- Shikanai T, Aro E-M. 2016. Evolution of photosynthetic NDH-1: structure and physiological function. In: Cramer W, Kallas T, eds. *Cytochrome complexes: evolution, structures, energy transduction, and signaling*. Dordrecht, the Netherlands: Springer Science + Business Media, 51–70.
- Sievers F, Wilm A, Dineen D, Gibson TJ, Karplus K, Li W, Lopez R, McWilliam H, Remmert M, Söding J *et al.* 2011. Fast, scalable generation of high-quality protein multiple sequence alignments using Clustal Omega. *Molecular Systems Biology* 7: 539.
- Stanier RY, Kunisawa R, Mandel M, Cohen-Bazire G. 1971. Purification and properties of unicellular blue-green algae (order *Chroococcales*). *Bacteriological Reviews* 35: 171–205.
- Thomas JC, Ughy B, Lagoutte B, Ajlani G. 2006. A second isoform of the ferredoxin: NADP oxidoreductase generated by an in-frame initiation of translation. *Proceedings of the National Academy of Sciences, USA* 103: 18368–18373.
- van Thor JJ, Mullineaux CW, Matthijs HCP, Hellingwerf KJ. 1998. Light harvesting and state transitions in Cyanobacteria. *Botanica Acta* 111: 430–443.
- Tyystjärvi E, Aro EM. 1996. The rate constant of photoinhibition, measured in lincomycin-treated leaves, is directly proportional to light intensity. *Proceedings of the National Academy of Sciences, USA* 93: 2213–2218.
- Yang C, Hua Q, Shimizu K. 2002. Metabolic flux analysis in *Synechocystis* using isotope distribution from <sup>13</sup>C-labeled glucose. *Metabolic Engineering* 4: 202–216.
- You L, Berla B, He L, Pakrasi HB, Tang YJ. 2014. 13C-MFA delineates the photomixotrophic metabolism of *Synechocystis* sp. PCC 6803 under light- and carbon-sufficient conditions. *Biotechnology Journal* 9: 684–692.
- You L, He L, Tang YJ. 2015. Photoheterotrophic fluxome in *Synechocystis* sp. strain PCC 6803 and its implications for cyanobacterial bioenergetics. *Journal of Bacteriology* 197: 943–950.
- Zhang P, Allahverdiyeva Y, Eisenhut M, Aro EM. 2009. Flavodiiron proteins in oxygenic photosynthetic organisms: photoprotection of photosystem II by Flv2 and Flv4 in *Synechocystis* sp. PCC 6803. *PLoS ONE* 4: e5331.
- Zhang P, Battchikova N, Jansen T, Appel J, Ogawa T, Aro EM. 2004. Expression and functional roles of the two distinct NDH-1 complexes and the carbon acquisition complex NdhD3/NdhF3/CupA/Sll1735 in *Synechocystis* sp. PCC 6803. *Plant Cell* 16: 3326–3340.

## Supporting Information

Additional Supporting Information may be found online in the Supporting Information tab for this article:

**Fig. S1** Effective yield of PS I Y(I) of the WT and the  $\Delta pntA$  mutant calculated from fluorescence analysis data.

Please note: Wiley Blackwell are not responsible for the content or functionality of any Supporting Information supplied by the authors. Any queries (other than missing material) should be directed to the *New Phytologist* Central Office.